energies

MDPI

Article

Application Characteristics of Zeolite-Based Stuffing for Nanofluidic Packer Rubber

Yafei Zhang [1,2,*], Jingwei Liang [1,2], Rui Luo [3], Shiwei Min [1,2] and Yihua Dou [1,2,*]

[1] School of Mechanical Engineering, Xi'an Shiyou University, Xi'an 710065, China
[2] Xi'an Key Laboratory of Wellbore Integrity Evaluation, Xi'an Shiyou University, Xi'an 710065, China
[3] Xi'an Thermal Power Research Institute Co., Ltd., Xi'an 710054, China
* Correspondence: effyzhang@126.com (Y.Z.); yhdou@vip.sina.com (Y.D.); Tel.: +86-134-8831-1584 (Y.Z.); +86-139-0918-3925 (Y.D.)

Abstract: Aiming at obtaining the application characteristics of more nanofluidic stuffing to enrich the database of nanofluidic packer rubber, three zeolite-based nanofluidic types of stuffing with water, glycerin, and a saturated aqueous solution of KCl (hereinafter referred to as saturated KCl solution) as the functional liquids were studied using experiments. The results showed that all the three zeolite-based nanofluidic stuffing types could be applied as stuffing for nanofluidic packer rubber. The setting pressure ranges for zeolite/water, zeolite/glycerin, and zeolite/saturated KCl solution stuffing were 21.71 to 30.62 MPa, 15.31 to 23.57 MPa, and 27.50 to 38.83 MPa, and the specific deformation quantities of the three stuffing types were 72.76, 102.07, and 77.54 $mm^3 \cdot g^{-1}$, respectively. In zeolite/saturated KCl solution stuffing, the number of liquid molecules retained in the nanochannels was the minimum; thus, this stuffing type was the most stable during application. The order of the equivalent surface tensions of the three zeolite-based stuffing types in the confined nanochannels was consistent with the order of the gas–liquid surface tensions in the bulk phase. The equivalent surface tension, which reflected the interaction between liquid–solid phases, dominated the pressure threshold, the deformation capacity, and the stability of nanofluidic stuffing. This research study provided data support for the application of nanofluidic packer rubber.

Keywords: packer rubber; nanofluidic stuffing; zeolite; pressure threshold; deformation capacity

Citation: Zhang, Y.; Liang, J.; Luo, R.; Min, S.; Dou, Y. Application Characteristics of Zeolite-Based Stuffing for Nanofluidic Packer Rubber. *Energies* **2022**, *15*, 7962. https://doi.org/10.3390/en15217962

Academic Editor: Xinpu Shen

Received: 13 September 2022
Accepted: 25 October 2022
Published: 27 October 2022

1. Introduction

The packer is an indispensable tool in oilfield operations that guarantees the normal production of oil exploration and the successful implementation of various down-hole operations. Packer rubber is the core component of the packer to seal the annulus and isolate the production layer [1]. At present, the exploitation of oil wells is developing towards deep/ultra-deep wells, and the corresponding harsh environment of high temperatures, high pressures, high corrosion, and complex strata put forward higher requirements for the performance of packer rubber. The aging [2] and stress relaxation [3] behaviors of rubber cylinders at high temperatures and under high pressures, the corrosion of formation water containing acid carbon dioxide [4] or the corrosion of seawater in deep-sea oilfields [5], the shell buckling of the large displacement horizontal part [6], the inhomogeneity of formation stress that leads to the uneven contact between packer rubber and the well wall [7], all greatly reduce the service life of packer rubber.

Researchers generally improved the performance of packer rubber in two aspects: one is the optimization of the structure, and the other is the improvement of the material. Zeng et al. [8] placed 15 steel strips with a thickness of 2 mm side by side inside rubber to obtain a large expansion packer, which could improve the sealing performance of the deformation sleeve. Wang et al. [9] found that the trapezoidal groove was the most proper shape for packer rubber, and the sealing property could be better when the bearing flow ring was installed inside the trapezoidal groove. Zhang et al. [10] determined the best structural

parameters of nylon cord rubber, which increased the load-bearing capacity of the packer by 25% and the sealing performance by 66%. Dong et al. [11] proposed a high-pressure sealing anti-shoulder (HPS-PSP) packer, which effectively solved the problems of hose shoulder protrusion and insufficient sealing performance. The contact pressure was 60.1% higher than that of traditional packers. Liu et al. [12] studied the mechanical behavior and sealing performance of packer rubber for different heights, thicknesses, external oblique angles, loading methods, and steel–rubber friction coefficients. Zheng et al. [13] optimized the thickness, height, and hardness parameters of the rubber cylinder. These improvements enhanced the sealing performance of packer rubber and later provided ideas for the structural design of packer rubber.

In addition to the optimization of the structure, the improvement of the rubber material is also a top priority. Nitrile rubber and its hydride are the main materials of rubber due to their excellent material properties. Others, such as fluorine rubber and polyurethane rubber, are also occasionally used [14]. Li et al. [15] tested the properties of hydrogenated nitrile rubber, fluorocarbon rubber, fluorosilicate rubber, and AFLAS rubber (tetrafluoroethylene-propylene rubber). The test results showed that for packer rubber used under high pressure conditions, such as fracturing or acid fracturing operations, the hydrogenated nitrile rubber material was recommended when the operating temperature was below 150 °C, and the fluorine rubber material was recommended when the operating temperature was above 150 °C. Gu et al. [16] developed high-quality packer rubber bearing 150 °C and 70 MPa by changing the rubber formula and production method. Liu [17] modified fluorine rubber (FKM) on the basis of its excellent anti-aging properties, improved its plasticity and thermal stability, and solved the problem of the poor long-term sealing performance of the rubber cylinder at high temperatures. He et al. [18] designed a rubber composite of hydrogenated nitrile rubber filled with carbon black and chopped aramid fibers, which could withstand high mechanical loads, high temperatures, and corrosive chemical media. Tong et al. [19] prepared Thermo-Plastic Vulcanizates (TPVs) using cheap Polyamide66 (PA66) instead of part of hydrogenated nitrile rubber (HNBR) and blending it with Porous Super Absorbent Resin (PSAR) and reinforced nanoparticles. The rubber material had high strength, heat resistance, and low cost. Zhang et al. [20] developed a degradable rubber material using a mixture of polyurethane and hydrogenated nitrile rubber as base rubber, which solved the problem of difficulty in unsealing after the fracturing of the ordinary rubber packer. Kleverlaan et al. [21] studied the sealing principles and application prospects of expandable elastomers and found that vulcanized rubber elastomers expanded when they came into contact with aromatic hydrocarbons or salt water and that expanded rubber played a major role in sealing the pipe string. Xu et al. [22] developed an elastic carbon composite material that could be used for ultra-deep downhole packers. It had excellent thermal stability above 538 °C and strong corrosion resistance to hydrocarbons and acids. Li et al. [23] prepared multi-walled carbon nanotube (MWCNT)-reinforced hydrogenated nitrile rubber (HNBR) composites to solve the key problem of the accelerated aging of packer cartridges at high temperatures.

Recently, a new type of packer rubber, nanofluidic packer rubber, was promoted by our team. The detailed description of the structure and working principle of the nanofluidic packer was published in our previous work [24]. Figure 1 shows the structure diagram of nanofluidic packer rubber. Nanofluidic packer rubber is composed of a honeycomb skeleton and nanofluidic stuffing. As the nanofluidic stuffing is a kind of suspension with no fixed form, the honeycomb structure was introduced as a skeleton to support and encapsulate the suspension. Nanofluidic stuffing is composed of a hydrophobic nanoporous medium and non-invasive functional liquids. In a nanofluidic system, only when the external pressure is great enough to overcome the capillary repulsion, the functional liquid molecules start entering the nanochannels and lead to an infiltration plateau in the ΔV-ΔP chart. The infiltration plateau of the nanofluidic stuffing is the ideal working range for nanofluidic packer rubber. During this working range, changes in annulus pressure or temperature trigger the flow of liquid molecules into or out of the nanochannels; then, the volume of

packer rubber changes, while the counterforce applied by packer rubber to the casing and tubing stabilize within a small range. The stress fluctuations and sealing failure of packer rubber are reduced as a consequence.

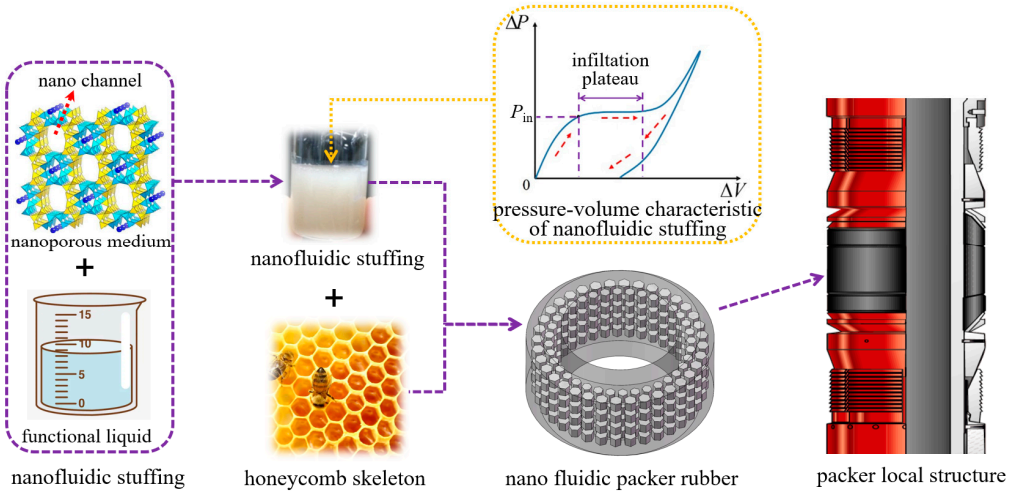

Figure 1. Structure diagram of nanofluidic packer rubber.

Nanofluidic stuffing is the core unit of nanofluidic packer rubber. By changing the formulation of nanofluidic stuffing, the system can possess different critical infiltration pressure (P_{in}) values and infiltration plateau ranges, so that nanofluidic packer rubber can deal with various complex downhole environments.

In the current study, three kinds of zeolite-based nanofluidic stuffing with different functional liquids were studied using experiments, and the operation characteristics of the nanofluidic stuffing for nanofluidic packer rubber were analyzed.

2. Experimental Preparation

ZSM-5 zeolite was selected as the nanoporous medium for nanofluidic stuffing. Water, glycerin, and saturated KCl solution were used as functional liquids separately. It should be noted that saturated KCl solution in this work refers to saturated aqueous solution of KCl at 30 °C. Thus, the three kinds of stuffing for the nanofluidic packer were ZSM-5 zeolite/water stuffing, ZSM-5 zeolite/glycerin stuffing, and ZSM-5 zeolite/saturated KCl solution stuffing. Raw ZSM-5 zeolite was purchased from Shanghai Fuxu Molecular Sieve Limited Company in China. Prior to the preparation of nanofluidic stuffing, the raw zeolite material was heated in a tube furnace at 600 °C for 6 h to remove impurities and improve stability. The pore volume of pretreated ZSM-5 zeolite was 510 $mm^3 \cdot g^{-1}$, and the pore size of the mesopore was around 2.114 nm. Then, pretreated ZSM-5 zeolite and the functional liquid, here referring to water, glycerin, or saturated KCl solution, were blended according to 1 g of zeolite to 10 mL of functional liquid. Then, we put the mixture in a vacuum environment for 12 h, to remove excessive air bubbles introduced in the previous blending step. Thus, nanofluidic stuffing was prepared.

During the experiments, nanofluidic stuffing was filled in a sealed pressure–volume test chamber. A stainless-steel rod was used as a piston, which could be moved upward and downward during the loading and unloading processes to change the volume in the chamber. With the decrease/increase in the volume inside the chamber, the pressure in the chamber increased/decreased. Due to the surface tension between the liquid and solid phases of nanofluidic stuffing, liquid molecules did not enter the nanochannels of zeolite until the pressure in the chamber reached a critical value. By recording the pressure inside the chamber and the displacement of the stainless-steel rod, we obtained the pressure–volume change characteristic of nanofluidic stuffing.

Figure 2 is a schematic diagram of the pressure–volume test bench for nanofluidic stuffing. A PLD-300 electro-hydraulic servo fatigue testing machine was used as loading–

unloading equipment of force. The pressure–volume test chamber of nanofluidic stuffing was composed of a stainless-steel chamber and a stainless-steel rod. An O-ring was used to seal the stainless-steel chamber and the stainless-steel rod. The PLD-300 testing machine controlled experimental parameters such as loading–unloading rate and numbers of loading–unloading cycles and recorded the displacement of the stainless-steel rod. A pressure sensor was embedded at the bottom of the stainless-steel rod; thus, the pressure change in nanofluidic stuffing in the test chamber could be monitored. During the experiments, the PLD-300 testing machine pressed down the stainless-steel rod to compress the nanofluidic stuffing in the stainless-steel chamber. When the pressure in the test chamber reached 50 MPa, it retrieved the stainless-steel rod at the same speed. After going back to the initial position, it pressed down the stainless-steel rod again to compress the nanofluidic stuffing. When the pressure in the test chamber reached 50 MPa, it retrieved the stainless-steel rod again. This process was repeated for ten successive loading–unloading cycles.

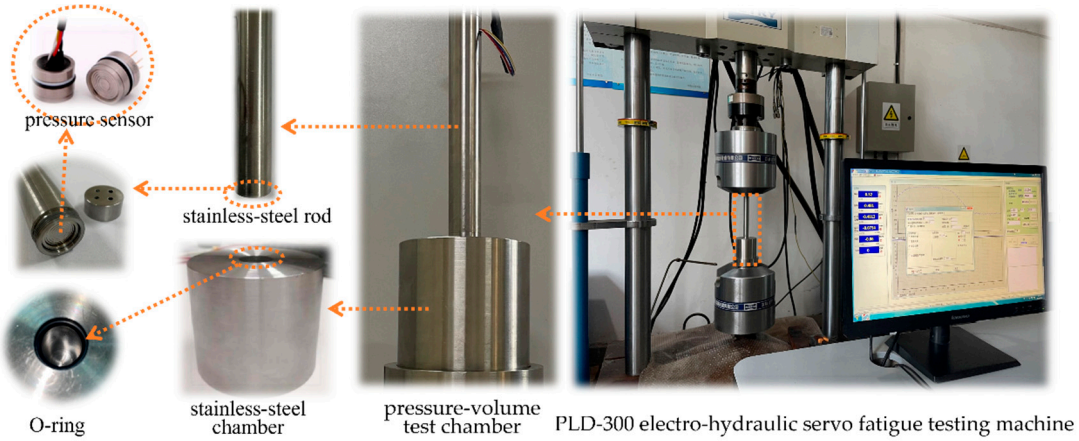

Figure 2. Pressure–volume test bench for nanofluidic stuffing.

3. Results and Discussion

3.1. Pressure-Specific Volume Curves of ZSM-5 Zeolite-Based Stuffing

Figure 3 shows the pressure-specific volume curves of the three zeolite-based stuffings at the loading rate of 0.02 mm·s^{-1}. We define the specific system volume change as $\Delta V = A\Delta d/m$, where A is the cross-sectional area of the stainless-steel rod, Δd is the rod's displacement, and m is the mass of zeolite.

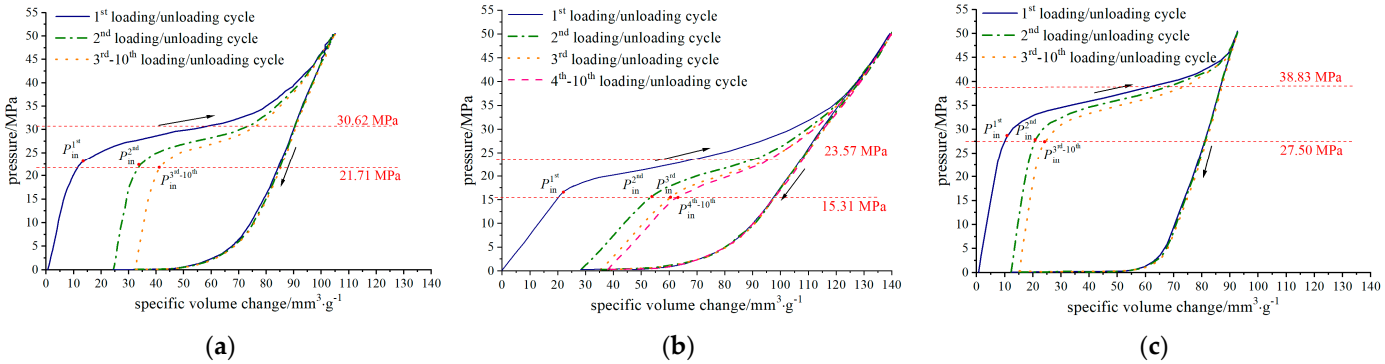

(**a**) (**b**) (**c**)

Figure 3. Pressure-specific volume curves of zeolite/water, zeolite/glycerin, and zeolite/saturated KCl solution stuffing (zeolite here refers to ZSM-5 zeolite, where zeolite and the functional liquid are blended according to 1 g to 10 mL): (**a**) zeolite/water stuffing; (**b**) zeolite/glycerin stuffing; (**c**) zeolite/saturated KCl solution stuffing.

As Figure 3 presents, during the loading period, when the pressure is relatively low, the functional liquid cannot enter the lyophobic zeolite pores due to the surface tension

between the solid and liquid phases. When the pressure reaches a critical value, P_{in}, the capillary repulsion is overcome, and pressure-induced infiltration occurs, forming a plateau region. Eventually, when the porous space is filled, the plateau region ends, and the system compressibility decreases significantly. When the pressure reaches about 50 MPa, the loading period ends. During the unloading period, the liquid molecules in the nanochannels are driven out by the hydrophobicity of the solid phase when the external pressure decreases.

In nanofluidic packer rubber, the plateau region during induced infiltration is the ideal working range. In this pressure plateau region, the volume of packer rubber decreases/increases as the liquid molecules enter/exit the nanochannels, and the fluctuations in both the external pressure and the annulus temperature are balanced by the system volume change, while the counterforce between rubber and tubing or between rubber and casing stabilizes in a small interval. The sealing performance of packer rubber is enhanced in consequence. The experimental results showed that all the three zeolite-based stuffing could work stably after the first few cycles. The pressure-specific volume curves of zeolite/glycerin stuffing overlapped from the fourth to the tenth loading–unloading cycles, while the pressure-specific volume curves of zeolite/water and zeolite/saturated KCl solution stuffing overlapped from the third loading–unloading cycle. In a stable working state, the setting pressure ranges for the zeolite/water, zeolite/glycerin, and zeolite/saturated KCl solution stuffing were 21.71 to 30.62 MPa, 15.31 to 23.57 MPa, and 27.50 to 38.83 MPa, respectively.

3.2. Pressure Threshold of ZSM-5 Zeolite-Based Stuffing

The infiltration critical pressure, P_{in}, is the pressure threshold of nanofluidic packer rubber. We define P_{in} (see Figure 3) as the first point around which the slope of the infiltration isotherm changes by more than 20% compared with the first leaner deformation stage before infiltration.

The pressure thresholds of the three kinds of zeolite-based stuffing were extracted from the pressure-specific volume change curves in Figure 3 and plotted in Figure 4. From Figure 4, we can see that the pressure threshold of zeolite/saturated KCl solution stuffing was the highest, followed by zeolite/water stuffing, and the zeolite/glycerin stuffing had the lowest. The molecular size of water is about 0.324 nm. The molecular size of glycerin is about 0.62 nm. Because of ionic hydration, a coating of approximately several molecular dimensions in thickness may form around K^+. The distance between the K-O bonds in KCl solution is about 0.28 nm [25]. In addition to the size of K^+, the size of the molecular group in KCl solution was the largest among the three kinds of functional liquid. In general, the larger the molecular size is, the greater the impetus required to push the molecules to intrude into the nanochannels is. However, the order of the pressure threshold of the three stuffing types did not match the order of the molecular/molecular group size of the three functional liquids. In nanofluidic stuffing, the pressure threshold is determined by the type and size of nanochannels, the property of the functional liquid, the interaction at the solid–liquid interface, and the conditions of the external environment. In the current study, the three kinds of nanofluidic stuffing were all ZSM-5 zeolite based; there were no differences in the type and size of nanochannels, and there were no changes in the conditions of the external environment. Thus, the difference in the pressure thresholds was mainly caused by the variety of the properties of functional liquids and the interaction at the solid–liquid interface. To further illuminate the interaction at the solid–liquid interface in the studied nanofluidic stuffing types, the equivalent surface tensions and contact angles at the solid–liquid interface of the three kinds of nanofluidic stuffing were calculated.

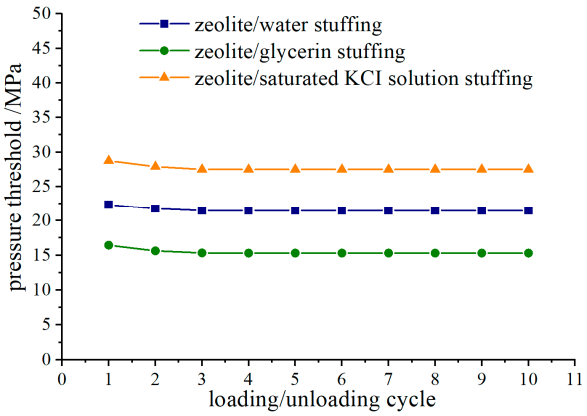

Figure 4. Pressure thresholds of the three kinds of zeolite-based stuffing under ten cyclic loadings (ZSM-5 zeolite/water stuffing, ZSM-5 zeolite/glycerin stuffing, and ZSM-5 zeolite/saturated KCl solution stuffing).

At the speed of 0.02 mm·s^{-1} under the experimental working conditions, the loading–unloading process could be regarded as quasi static [24], and the loading rate effect was negligible. We employed the classic Young's equation to relate the pressure threshold, P_{in}, to the pore size, d: $P_{in} = 4\overline{\gamma}/d$, where $\overline{\gamma}$ is the equivalent surface tension and d is the pore size of porous medium. The contact angle, α, conforms to $\cos\alpha = (\gamma_{sa} - \gamma_{sl})/\gamma_{la}$, where $\gamma_{sa} - \gamma_{sl}$ is the equivalent surface tension $\overline{\gamma}$ and γ_{la} is the surface tension of the gas–solid interface, which varies with the variety of the solution, and can be obtained from the research results in references [26,27]. The value of P_{in} is taken from the pressure-specific volume curve; thus, the equivalent surface tension, $\overline{\gamma}$, and the contact angle, α, of nanofluidic stuffing can be calculated.

Figure 5a,b show the equivalent surface tensions and contact angles of the three kinds of nanofluidic stuffing under ten loading–unloading cycles. It can be seen from the figures that the equivalent surface tensions and contact angles decreased slightly during the first three loading–unloading cycles and stayed around a certain value from the third to the tenth cycles. In the confined nanofluid environment, the order of the equivalent surface tensions of the three kinds of nanofluidic stuffing was consistent with the order of the classic gas–liquid surface tensions of the three liquids at large solid surfaces. The equivalent surface tension, which indicated the interaction between the liquid–solid phases, dominated the pressure threshold of nanofluidic stuffing.

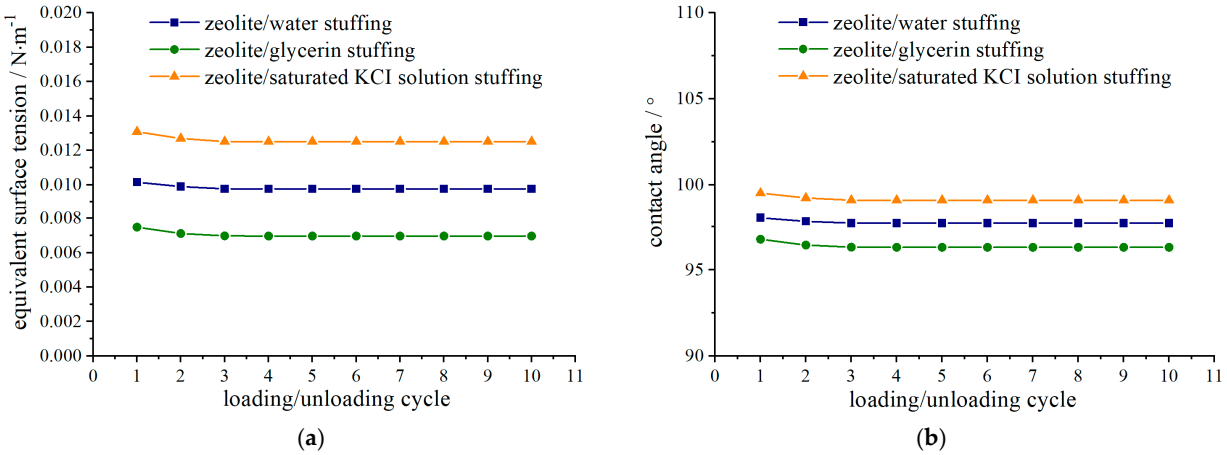

Figure 5. Equivalent surface tension and contact angle of three kinds of zeolite-based stuffing under ten cyclic loadings (ZSM-5 zeolite/water stuffing, ZSM-5 zeolite/glycerin stuffing, and ZSM-5 zeolite/saturated KCl solution stuffing): (**a**) equivalent surface tension; (**b**) contact angle.

3.3. Deformation Capacity of ZSM-5 Zeolite-Based Stuffing

The deformation capacity of nanofluidic packer rubber could be characterized using the specific deformation quantity of nanofluidic stuffing. Figure 6 plots the specific deformation quantities per mass of zeolite for the three kinds of stuffing when the external pressure reached 50 MPa. During the first loading–unloading cycle, the deformation quantity of zeolite/glycerin stuffing was the largest, followed by zeolite/water stuffing, and the smallest was that of zeolite/saturated KCl solution stuffing. This indicated that ZSM-5 zeolite permitted the largest access pore volume for glycerin molecules during the loading process. The main reason was that the equivalent surface tension of zeolite/glycerin stuffing was the lowest (see Figure 5a). Not only it caused glycerin molecules to encounter less resistance when entering the nanochannels, but it also led to a smaller repulsive force on glycerin molecules while transferring in the nanochannels. Therefore, glycerin molecules entered at the deepest depth, and the specific deformation quantity of zeolite/glycerin stuffing was the largest. In the successive two/three loading–unloading cycles, the deformation quantities of the tested stuffing all decreased significantly compared with the deformation quantities during the first loading–unloading cycle. The decline rates of the deformation quantities of zeolite/water and zeolite/glycerin stuffing were greater than that of zeolite/saturated KCl solution stuffing. After the fourth loading–unloading cycle, the specific deformation quantities of zeolite/water, zeolite/glycerin, and zeolite/saturated KCl solution stuffing were stable at 72.76, 102.07, and 77.54 $mm^3 \cdot g^{-1}$, respectively.

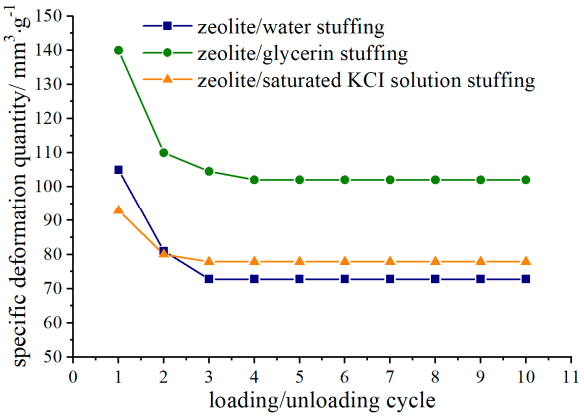

Figure 6. Specific deformation quantity of three kinds of zeolite-based stuffing under ten cyclic loadings (ZSM-5 zeolite/water stuffing, ZSM-5 zeolite/glycerin stuffing, and ZSM-5 zeolite/saturated KCl solution stuffing).

In this work, the defiltration percentage is defined as the ratio of the infiltration volume of the subsequent cycle to the maximum accessible infiltration volume. The infiltration volume of the first loading–unloading cycle is assumed to be the maximum accessible infiltration volume of zeolite. The defiltration percentage is an important parameter characterizing the throughput capacity of nanofluidic stuffing and can be used to evaluate the stability of nanofluidic stuffing during application. Figure 7 shows the defiltration percentages of the three kinds of zeolite-based stuffing under ten loading–unloading cycles. The defiltration percentage of nanofluidic stuffing is also closely related to the equivalent surface tension. As mentioned above, when the repulsive force of the solid wall decreased, the depth of intrusion increased. Yet, correspondingly, the driving force for liquid molecules to exit the pores during the outflow process applied by the solid wall decreased. Because the equivalent surface tension of zeolite/glycerin stuffing was the lowest among the three, glycerin molecules were more inclined to remain trapped in the pores of the porous medium, which led to a low defiltration percentage.

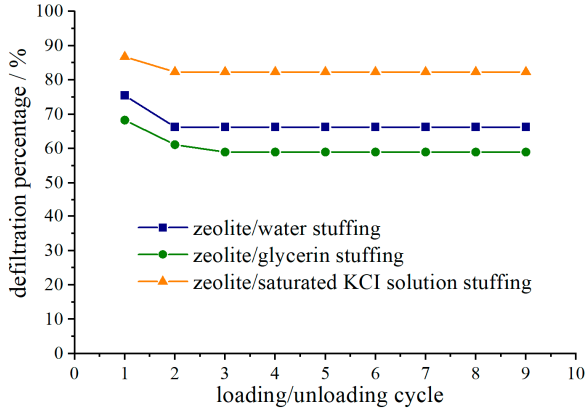

Figure 7. Defiltration percentage of three kinds of zeolite-based stuffing under ten cyclic loadings (ZSM-5 zeolite/water stuffing, ZSM-5 zeolite/glycerin stuffing, and ZSM-5 zeolite/saturated KCl solution stuffing).

Note that as the existence of defects in the nanochannels structures and the retention of liquid molecules, the deformation quantity during the loading process cannot be completely recovered after unloading. Corresponding to Figure 3, the unloading curve could not go back to the initial position when the pressure went back to 0 MPa during the first few loading–unloading cycles. However, the retention of liquid molecules is not permanent and can be released under certain conditions. As studied in our previous work, with the increase in the system temperature, the wettability at solid–liquid interface changes; the trapped liquid molecules may escape from the nanochannels, and the deformation capacity of nanofluidic stuffing is improved [28]. As is shown in Figure 7, in the first few loading–unloading cycles, the defiltration percentage decreased with the cycle number. For the same nano porous medium, the structure defects are basically the same, and the difference in defiltration percentage is mainly caused by the difference in the amount of retained liquid molecules. The decline rate of the defiltration percentage of zeolite/saturated KCl solution stuffing was the smallest. It indicated that the number of liquid molecules retained in the nanochannels was the minimum among the studied stuffing types. As a result, the system parameters of zeolite/saturated KCl solution stuffing were the most stable when the downhole temperature fluctuated.

4. Conclusions

Nanofluidic packer rubber, composed of nanofluidic stuffing and a honeycomb skeleton, possesses the advantage of the pressure-specific volume change characteristic of nanofluidic stuffing. In the current study, ZSM-5 zeolite/water, ZSM-5 zeolite/glycerin, and ZSM-5 zeolite/saturated KCl solution stuffing types were studied using experiments, and the operation characteristics of nanofluidic stuffing for nanofluidic packer rubber were analyzed.

The results showed that all the three kinds of zeolite-based nanofluidic stuffing could be applied as stuffing for nanofluidic packer rubber. The studied stuffing types could reach a throughput balance after two/three loading–unloading cycles. The setting pressure ranges for zeolite/water, zeolite/glycerin, and zeolite/saturated KCl solution stuffing were 21.71 to 30.62 MPa, 15.31 to 23.57 MPa, and 27.50 to 38.83 MPa, and the specific deformation quantities of zeolite/water, zeolite/glycerin, and zeolite/saturated KCl solution stuffing were 72.76, 102.07, and 77.54 $mm^3 \cdot g^{-1}$, respectively.

In the confined nanofluid environment, the order of the equivalent surface tensions of the three kinds of nanofluidic stuffing was consistent with the order of the gas–liquid surface tensions of the three liquids in the bulk phase. Comparing with the size of liquid molecules, the equivalent surface tensions acted more on the pressure thresholds of nanofluidic stuffing. The equivalent surface tension of zeolite/glycerin stuffing was the lowest among the three. Thus, its deformation quantity was the largest, and its defiltration percentage

was the lowest. The pressure threshold of zeolite/saturated KCl solution stuffing was higher than that of zeolite/water stuffing. In zeolite/saturated KCl solution stuffing, the number of liquid molecules retained in the nanochannels was the minimum; thus, the system parameters of this type stuffing were the most stable when the downhole temperature fluctuates.

Nanofluidic packer rubber is composed of a honeycomb skeleton and nanofluidic stuffing. Although nanofluidic stuffing dominates the volume change characteristic of packer rubber, the structure and material of the honeycomb skeleton also influence the mechanical properties of packer rubber. The experimental data obtained in the current work can be used as reference in the design of nanofluidic packer rubber. For the mechanical property of nanofluidic packer rubber, nanofluidic stuffing and the honeycomb skeleton should be taken as integral parts to be further studied.

Author Contributions: Conceptualization, Y.Z. and Y.D.; methodology, Y.Z. and R.L.; validation, J.L., R.L. and S.M.; formal analysis, R.L. and S.M.; investigation, J.L.; resources, R.L.; data curation, J.L.; writing—original draft preparation, Y.Z.; writing—review and editing, J.L.; supervision, Y.D.; project administration, Y.D.; funding acquisition, Y.Z. All authors have read and agreed to the published version of the manuscript.

Funding: This research study was funded by National Natural Science Foundation of China (grant No. 51974246), Innovative Talent Promotion Program "Young Science and Technology Star Project" of Shaanxi Province of China (grant No. 2021KJXX-40), and Natural Science Foundation of Shaanxi Province of China (grant No. 2020JM-538).

Data Availability Statement: Not applicable.

Conflicts of Interest: The authors declare no conflict of interest.

References

1. Ma, W.; Qu, B.; Guan, F. Effect of the friction coefficient for contact pressure of packer rubber. *Proc. Inst. Mech. Eng. Part C J. Mech. Eng. Sci.* **2014**, *228*, 2881–2887. [CrossRef]
2. Dong, L.; Li, K.; Zhu, X.; Li, Z.; Zhang, D.; Pan, Y.; Chen, X. Study on high temperature sealing behavior of packer rubber tube based on thermal aging experiments. *Eng. Fail. Anal.* **2020**, *108*, 104321. [CrossRef]
3. Zheng, X.; Li, B. Study on sealing performance of packer rubber based on stress relaxation experiment. *Eng. Fail. Anal.* **2021**, *129*, 105692. [CrossRef]
4. Zhu, D.; Lin, Y.; Zhang, H.; Li, Y.; Zeng, D.; Liu, W.; Qiang, C.; Deng, K. Corrosion evaluation of packer rubber materials in CO_2 injection wells under supercritical conditions. *J. Pet. Sci. Eng.* **2017**, *151*, 311–317. [CrossRef]
5. Zhu, X.; Liu, B. The reliability-based evaluation of casing collapsing strength and its application in marine gas reservoirs. *Eng. Fail. Anal.* **2018**, *85*, 1–13. [CrossRef]
6. Xi, Y.; Li, J.; Liu, G.; Cha, C.; Fu, Y. Numerical investigation for different casing deformation reasons in Weiyuan-Changning shale gas field during multistage hydraulic fracturing. *J. Pet. Sci. Eng.* **2018**, *163*, 691–702. [CrossRef]
7. Chen, B.; Ding, G.; Fei, G.; Shen, H.; Wang, X. Influence of irregular wellbore shape on sealing performance of packer. *Chin. J. Appl. Mech.* **2021**, *38*, 1127–1134. (In Chinese)
8. Zeng, S.; Zhang, Z. The analysis of compound packer rubber. *Appl. Mech. Mater.* **2013**, *271–272*, 1160–1163. [CrossRef]
9. Wang, H.; Chen, S.; Liu, Y.; Zhang, L.; Zhang, Z. Numerical simulation and experimental validation for design improvement of packer rubber. *Int. J. Simul. Process Model.* **2017**, *12*, 419–428. [CrossRef]
10. Zhang, Y.; Wang, H.; Che, J.; Du, M.; Zhang, H. Multi-objective optimization and experiment of nylon cord rubber in expandable packer. *Pet. Sci.* **2021**, *18*, 269–284. [CrossRef]
11. Dong, L.; Li, K.; Li, B.; Zhu, X.; Xie, M.; Zhang, Y.; Wang, J. Study in deep shale gas well to prevent shoulder protruding packer with high pressure sealing. *Eng. Fail. Anal.* **2020**, *118*, 104871. [CrossRef]
12. Liu, J.; Deng, K.; Liu, S.; Yan, X.; Li, L.; Zou, D.; Lin, Y. Mechanical behavior and structure optimization of compressed PHP packer rubber. *J. Mater. Eng. Perform.* **2021**, *30*, 3691–3704. [CrossRef]
13. Zheng, C.; Zheng, X.; Qin, J.; Liu, P.; Aibaibu, A.; Liu, Y. Nonlinear finite element analysis on the sealing performance of rubber packer for hydraulic fracturing. *J. Nat. Gas Sci. Eng.* **2021**, *85*, 103711. [CrossRef]
14. Xu, Z.; Zhang, Y.; Li, A.; Wang, J.; Wang, G.; He, Q. Research progress on compounding agent and mechanical test method of fluororubber. *J. Appl. Polym. Sci.* **2021**, *138*, 50913.
15. Li, S.; Ge, J.; Yin, Q.; Shi, S.; Xu, G.; Zhao, Q. Effect of corrosive environment in gas well on cartridge rubber material of packer. *Surf. Technol.* **2018**, *47*, 51–59. (In Chinese)

16. Gu, D.; Liu, G.; Chai, C.; Liu, J.; Pan, S.; Bai, Y.; Wang, W. Properties Research of Packer Rubber Materials. In Proceedings of the International Conference on Power Engineering & Energy Environment (PEEE 2016), Shanghai, China, 25–26 June 2016.
17. Liu, Y. The development and field testing of a high-temperature deep-layer open hole packer for acid fracturing completion in deep carbonate reservoirs. *Pet. Drill. Tech.* **2020**, *48*, 76–81. (In Chinese)
18. He, X.; Shi, X.; Hoch, M.; Gögelein, C. Mechanical properties of aramid fiber and carbon black filled hydrogenated nitrile rubber for packer compounds. *Polym. Compos.* **2018**, *39*, 3212–3226. [CrossRef]
19. Tong, Z.; Ye, Q.; Qian, J.; Hao, Z.; Wang, L. Down-hole isolation towards high-temperature reservoir using packing elements with swellable thermo-plastic vulcanizates. *J. Pet. Sci. Eng.* **2019**, *172*, 964–975. [CrossRef]
20. Zhang, Y.; Li, J.; Yang, X.; Zhang, W.; Liu, X.; Wang, M. New degradable fracturing packer rubber. *Well Testing* **2019**, *28*, 51–55. (In Chinese)
21. Kleverlaan, M.; van Noort, R.H.; Jones, I. Deployment of swelling elastomer packers in Shell E&P. In Proceedings of the SPE/IADC Drilling Conference, Amsterdam, The Netherlands, 23–25 February 2005.
22. Xu, Z.; Zhao, L.; Ganguly, P. Elastic carbon composite and its use as ultrahigh temperature packer element. In Proceedings of the SPE Middle East Oil & Gas Show and Conference, Manama, Kingdom of Bahrain, 6–9 March 2017.
23. Li, H.; Cheng, K.; Zhang, Z.; Zhao, L.; Zhou, H.; Wang, H.; Li, Z. Effect of carbon nanotubes on aging properties of hydrogenated nitrile rubber in the dilute oxygen medium. *J. Macromol. Sci. Part A.* **2022**, *59*, 38–45.
24. Dou, Y.; Zhang, Y.; Liang, J.; Chao, R. Experimental study on application characteristics of zeolite/water stuffing for the nanofluidic packer rubber. *Adv. Mech. Eng.* **2020**, *12*, 1687814020971901. [CrossRef]
25. Bankura, A.; Carnevale, V.; Klein, M.L. Hydration structure of salt solutions from ab initio molecular dynamics. *J. Chem. Phys.* **2013**, *138*, 014501. [CrossRef]
26. Jarvis, N.L.; Scheiman, M.A. Surface potentials of aqueous electrolyte solutions. *J. Phys. Chem.* **1968**, *72*, 74–78. [CrossRef]
27. Gallant, R.W. Physical properties of hydrocarbons. *Hydrocarb. Process.* **1967**, *46*, 119–125.
28. Zhang, Y.; Li, N.; Luo, R.; Zhang, Y.; Zhou, Q.; Chen, X. Experimental study on thermal effect on infiltration mechanisms of glycerin into ZSM-5 zeolite under cyclic loadings. *J. Phys. D Appl. Phys.* **2015**, *49*, 025303. [CrossRef]